Materials Horizons

ROYAL SOCIETY
OF CHEMISTRY

COMMUNICATION
Arri Priimagi, Yan Jun Liu *et al.*
Photoelastic plasmonic metasurfaces with ultra-large near
infrared spectral tuning

ROYAL SOCIETY
OF CHEMISTRY

COMMUNICATION

Check for updates

Photoelastic plasmonic metasurfaces with ultra-large near infrared spectral tuning†

Jianxun Liu, ‡[a] Hao Zeng, ‡[b] Ming Cheng, [a] Zhenming Wang,[a] Jiawei Wang,[a] Mengjia Cen,[a] Dan Luo, [a] Arri Priimagi *[b] and Yan Jun Liu *[ac]

Metasurfaces, consisting of artificially fabricated sub-wavelength *meta*-atoms with pre-designable electromagnetic properties, provide novel opportunities to a variety of applications such as light detectors/sensors, local field imaging and optical displays. Currently, the tuning of most metasurfaces requires redesigning and reproducing the entire structure, rendering them ineligible for post-fabrication shape-morphing or spectral reconfigurability. Here, we report a photoelastic metasurface with an all-optical and reversible resonance tuning in the near infrared range. The photoelastic metasurface consists of hexagonal gold nanoarrays deposited on a deformable substrate made of a liquid crystalline network. Upon photo-actuation, the substrate deforms, causing the lattice to change and, as a result, the plasmon resonance to shift. The centre wavelength of the plasmon resonance exhibits an ultra-large spectral tuning of over 245 nm, from 1490 to 1245 nm, while the anisotropic deformability also endows light-switchable sensitivity in probing polarization. The proposed concept establishes a light-controlled soft platform that is of great potential for tunable/reconfigurable photonic devices, such as nano-filters, -couplers, -holograms, and displays with structural colors.

New concepts

Conventional plasmonic metasurfaces are fabricated on rigid substrates using accurate nanofabrication tools for controlling the spatial location of the individual nano-antennae, which cannot be post-modified after fabrication. Actively tunable metasurfaces with reversible control over the lateral distance of the nano-antennae have been obtained by using soft, mechanically deformable substrates, requiring physical contact between the metasurface and the stimulus source. Herein we present a route towards remote, reversible control over the plasmon resonances in response to light stimulus. Our concept is based on hexagonal gold nano-arrays deposited on a light-responsive liquid crystal network substrate, yielding a photoelastic metasurface with ultra-large, 245 nm tuning of the plasmon resonance in the near infrared range. The light-induced deformation of the substrate is anisotropic, which endows light-switchable polarization dependence of the resonance wavelength and transmittance of the metasurface. This study serves to demonstrate that plasmonic metasurfaces can be elastic and photo-tunable, while from the other perspective, soft robotic materials such as liquid crystal networks can be designed to possess photonic functionalities. Hence, it acts as a bridge aiming to connect the disciplines of photonics and soft robotics.

Introduction

Plasmonic metasurfaces have received a great deal of attention in photonics, due to their unique ability to abruptly change the

*a Department of Electrical and Electronic Engineering, Southern University of
Science and Technology, Shenzhen 518055, China. E-mail: yjliu@sustech.edu.cn,
liujx@sustech.edu.cn, 12051010@mail.sustech.edu.cn,
11510868@mail.sustech.edu.cn, 11930844@mail.sustech.edu.cn,
cenmengjia@mail.dlut.edu.cn, luod@sustech.edu.cn; Tel: +86 755 8801 8520*

*b Smart Photonic Materials, Faculty of Engineering and Natural Sciences, Tampere
University, P.O. Box 541, Tampere FI-33101, Finland.
E-mail: arri.priimagi@tuni.fi, hao.zeng@tuni.fi; Tel: +358 44 515 0300*

*c Key Laboratory of Energy Conversion and Storage Technologies (Southern
University of Science and Technology), Ministry of Education, Shenzhen 518055,
China*

† Electronic supplementary information (ESI) available. See DOI: 10.1039/
d1mh01377g

‡ These authors contributed equally.

amplitude, phase and polarization of a propagating light beam.[1–4] Through localized surface plasmon resonances, metasurfaces allow for sophisticated control over the light-matter interactions, serving as a design tool for potential applications in the fields of beam manipulation,[5] flat lenses,[6] nano-holography,[7] biosensing,[8] and color printing.[9] For future applications towards adaptive optics and tunable photonic devices, there is a strong need to reversibly control the plasmonic signals.[10–18] However, to date most of the metasurfaces are made of undeformable materials and fabricated on rigid substrates, posing great hurdles for post-modification of their properties after fabrication.

Thanks to the extensive research on stimuli-responsive materials, such as phase-change materials, electro- and magneto-optical materials, and liquid crystals, various active metasurfaces have been reported.[10,19,20] Modulated metasurfaces for tunable absorption,[21] beam steering,[22,23] varifocal metalenses,[24] and ultrafast optical nonlinearity[25] have been

demonstrated, holding great potential for applications in tunable photonics. For conventional phase-changing materials based on modification of the refractive index of the substrate or the medium around the plasmonic units,[26–30] it is challenging to obtain large spectral tuning range due to limited refractive-index changes and optical losses. Another effective strategy towards active metasurfaces is positioning the metasurface onto mechanically deformable substrate.[31] Mechanical deformation can directly deform the lattice periodicity of the *meta*-atoms, and is hence deemed as an efficient approach for active metasurfaces for spectral tuning,[32] structural colors,[33] varifocusing,[34] dynamic holography,[35] and so on. Several metasurfaces fabricated on soft substrates exhibit spectral tuning upon externally applied strain through mechanical stretching.[33,36,37] To exclude the cumbrous physical contact for obtaining the deformation and to miniaturize the system size for further optoelectronic integration, active metasurfaces possessing mechanical deformability that can be controlled with remote stimuli would be strongly desired.

Liquid crystal networks (LCNs)[38–40] are a class of smart materials that can undergo large deformation in response to stimuli such as electric,[41] magnetic,[42] and light[43] fields. Combining elasticity arising from the polymer network and anisotropy given by liquid crystal orientation, LCNs can perform reversible deformation and versatile shape-morphing, being an attractive material platform for artificial muscles and soft micro-robotics.[44–46] From the viewpoint of photonics, the reversible photomechanical deformability and order-to-disorder phase transition of the LCN (which is accompanied by large change in refractive index) are promising routes towards reconfigurable devices.[47–50] Yet only few LCN-based micro- or nanophotonic structures have been reported. They serve as early examples of optical control over reflectance,[43]

diffraction,[50] interference colour,[51] and optical resonator.[52] However, the small light extinction cross-section of these LCN-based photonic elements has restricted the ability of modulation in spectrum. It is expected that a hybridization between the largely deformable LCNs with metasurfaces with high light extinction cross-section could yield more efficient tuning of resonances through photomechanical actuation.

Here, we report a method to realize photoelastic metasurfaces with reversible tuning of the localized surface plasmon resonance (LSPR). The plasmon resonance is given by a gold nanoarray fabricated on top of a light-deformable LCN substrate *via* nanosphere lithography. Optically induced lateral deformation of the elastic substrate endows spectral tuning across 245 nm in the near-infrared regime, and light-switchable polarization sensitivity driven by lateral deformation anisotropy. We provide in-depth characterization of the continuous tuning performance and actuation kinetics of the photoelastic metasurfaces. We also demonstrate temporal control over light diffraction patterns, to show the potential of realizing all-optical control for future tunable photonics.

Results

System concept

Fig. 1a shows the schematics of the tunable photoelastic metasurface, in which the hexagonal Au nanostructure is deposited on a photo-deformable LCN substrate. The Au pattern was fabricated using nanosphere lithography (NSL),[53,54] where a monolayer of self-assembled polystyrene (PS) nanospheres was used as a deposition mask. After the gold deposition process with an electron-beam evaporator, the PS nanosphere mask was removed by sonication in deionized
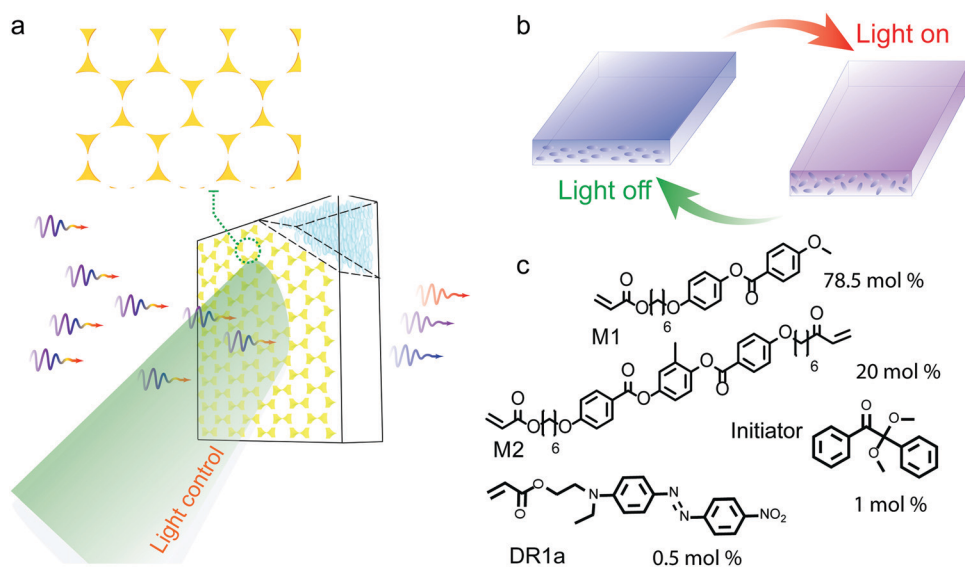

Fig. 1 The concept of photoelastic metasurface. (a) Schematics of the plasmonic metasurface fabricated *via* nanosphere lithography. (b) Schematic drawing of the photomechanical LCN substrate undergoing reversible shape-change upon light excitation. (c) The chemical structures of the constituents of the LCN used.

water. Eventually, the hexagonally distributed nanoarray was fabricated on the LCN surface, as schematized in Fig. 1a. Further details on the fabrication process are given in Methods and in ESI† Fig. S1.

An LCN substrate with planar molecular alignment can exhibit reversible deformation upon photothermal excitation,[40] as illustrated in Fig. 1b. Upon excitation, the uniaxially aligned molecules (due to polymerization in aligned nematic LC phase) undergo phase transition into isotropic phase, thus destroying the molecular orientation that is originally preserved by the crosslinked network. This order-to-disorder phase transition yields macroscopic deformation of the whole substrate.[55] The shape-change occurs in all directions: the sample contracts along the LC director and expands in the perpendicular lateral direction and in the thickness direction. This shape change will accordingly reshape the Au lattice geometry fabricated on top of the substrate. A commercially available monomer mixture is used to compose the LCN substrate (Fig. 1c). Dispersed Red 1 acrylate (DR1a) is chemically linked to the polymer network as a photothermal agent, to transfer the light energy

into heat generation.[46] The absorption spectra and polarized optical images of the LCN are shown in ESI† Fig. S2 and S3, respectively. The photomechanical actuation strategy that we implement is as follows: when the LCN substrate is irradiated with a continuous-wave laser with wavelength of 532 nm, the uniaxial molecular orientation is disrupted due to photothermal heating. This causes anisotropic lateral deformation, which results in reconfiguration of the periodicity of the metasurface and shifts the plasmon resonance. After ceasing the light irradiation, the elasticity of the LCN restores the original geometry and the resonance is expected to shift back to the original spectral position.

Au nanoarray and deformable substrate

Scanning electron microscope (SEM) imaging (Fig. 2a on LCN surface and ESI† Fig. S4 on glass substrate) reveals that high-quality Au nanoarrays can be obtained over a large area. As 1 μm diameter PS spheres are used, the hexagonal structure yields a lattice constant of 577 nm in one supercell (denoted as *d* in Fig. 2b). The details about the arc edge of the nanotriangles
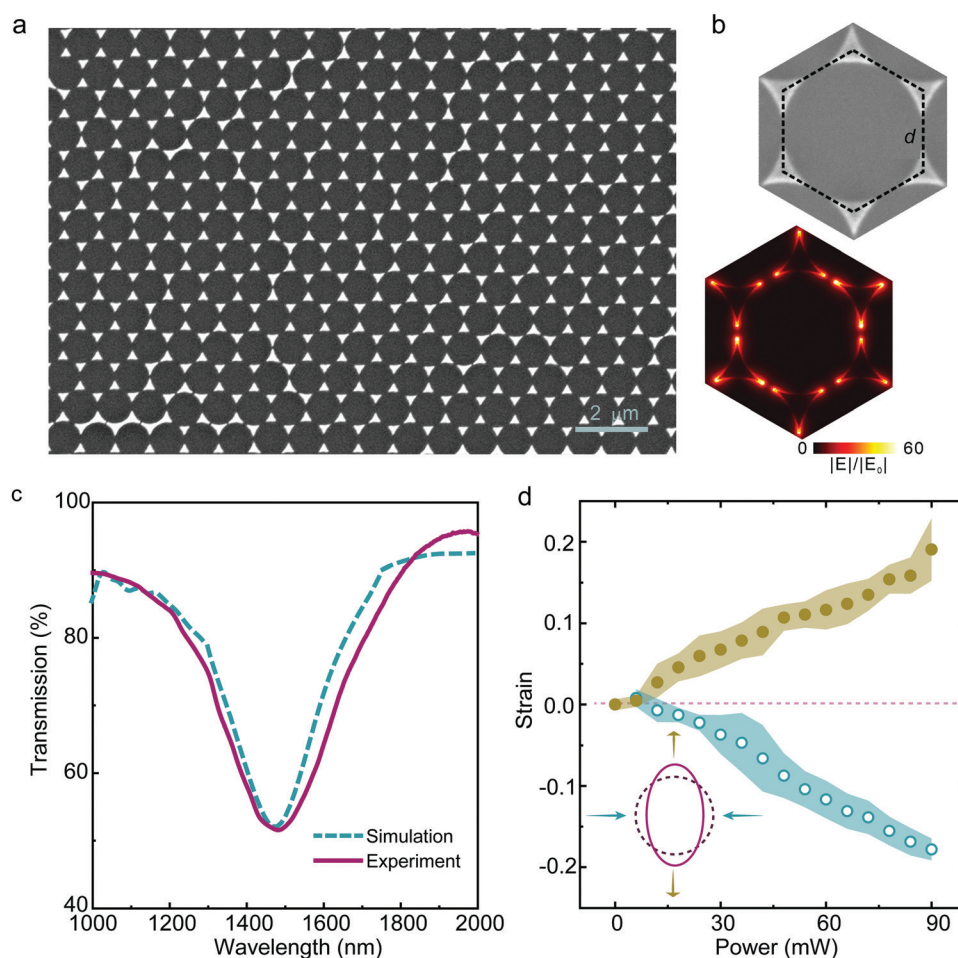

Fig. 2 Plasmon resonances of the photoelastic metasurface. (a) SEM image of the Au nanoarray on the LCN surface. (b) SEM image of one supercell of the hexagonally distributed nanotriangles and its calculated field enhancement. The dotted hexagon represents the boundary of the supercell. (c) Simulated and measured transmission spectra of the Au nanoarray on the LCN with unpolarized incident light. (d) Anisotropic deformation of the LCN substrate (negative value for contraction and positive for expansion) upon irradiation with 532 nm laser.

are shown in the SEM image in ESI† Fig. S5a. The thickness of the Au nano-objects is 50 nm, as measured by atomic force microscope (ESI† Fig. S5b and c). A finite-difference time-domain (FDTD) method is used to simulate the plasmon resonance, the details of which are given in ESI.† The refractive index of the LCN substrate is measured by a spectroscopic ellipsometer as shown in ESI† Fig. S6. Indicated by the simulation results, the electromagnetic field distribution in one super-cell exhibits an LSPR-induced field enhancement – as defined by $|E|/|E_0|$ (magnitude of the electric field/the incident field magnitude) – of *ca.* 60 at the tips of the nanotriangles (Fig. 2b). Fig. 2c shows the simulated and experimentally measured transmission spectra of the Au nanoarray on an LCN substrate, both showing resonance wavelengths at 1490 nm. The slight mismatch between the experimental and simulated results is ascribed to fabrication defects arising especially during the self-assembly of the PS nanospheres and the ultrasonic cleaning process.

The LCN substrate undergoes heat-induced deformation as characterized in ESI† Fig. S7. Light-induced heating can also trigger efficient deformation, causing about 20% contraction along the director axis and similar expansion in the perpendicular directions (Fig. 2d). The photoelastic deformation is fully reversible after cooling to room temperature. Since the Au nanoarray is fabricated with strict lattice geometry on top of an anisotropic substrate, the resonance wavelength and extinction ratio are sensitive to the refractive index of the substrate and the periodicity of the nanotriangles,[56,57] which both change during the photothermal deformation. Therefore, the photoelastic metasurface is expected to yield large spectral shift in the resonance, which will be proven in the following sections.

Tuning of plasmon resonances on the photoelastic metasurface

After fabricating the Au nanoarray on the LCN substrate, the resonance wavelength is centered around 1490 nm with unpolarized light incidence, as shown in Fig. 3a. By gradually elevating the excitation power, the supercell lattice of the Au nanoarray is reduced along the orientation direction and enlarged in the perpendicular direction as schematically indicated in the insert of Fig. 3a. As a result, the resonance (center wavelength of the transmission dip) is continuously shifted from 1490 to 1245 nm (Fig. 3a), and the full width at half-maximum (FWHM) of the transmission dip increases from 421 nm to 485 nm. The refractive index of the LCN is estimated with a spectroscopic ellipsometer (ESI† Fig. S6). Both the
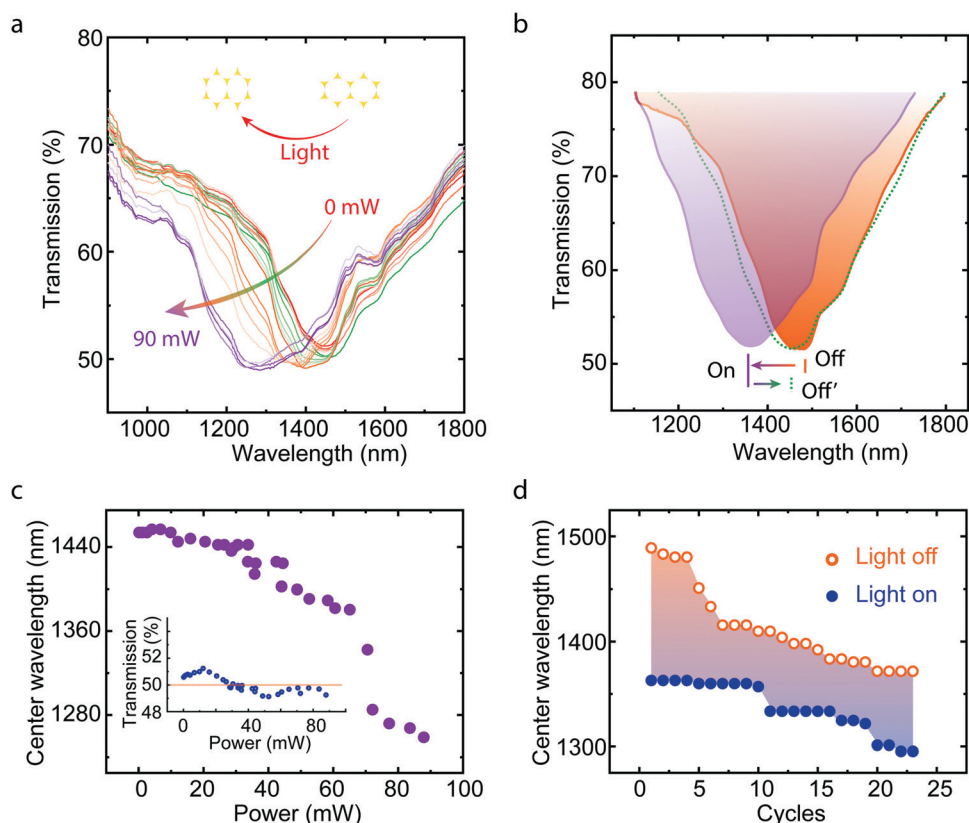

Fig. 3 Photomechanical tuning of plasmon resonances. (a) Transmission spectra shifting upon increasing the laser excitation power. Inset: Schematics of the deformation for two neighboring pairs of nanotriangle supercells. (b) Spectral change after one excitation cycle. (c) The resonance wavelength and transmittance (inset) as a function of excitation intensity. (d) The resonance wavelength upon cyclic light excitation. Excitation conditions in (a and c): laser power raises from 0 to 90 mW with step of 3 mW. In (b and d): for each excitation cycle, the laser is turned on and off for 1 min, and the laser power is 60 mW. Spot size is 700 μm.

extraordinary refractive index n_e and the ordinary one, n_o, change upon light excitation, as evidenced by the loss of birefringence ($\Delta n = n_e - n_o$) in the polarized optical micrographs (ESI† Fig. S8). An FDTD simulation is conducted by using the measured birefringence and an average refractive index $\langle n_{eff}^2 \rangle = (n_e^2 + 2n_o^2)/3$[58,59] to approximate the isotropic state of the LCN, showing good consistency between the experimental results and the simulation (ESI† Fig. S9). Compared to the modest spectral shifting upon changing the refractive index without any mechanical deformation (ESI† Fig. S10), one can conclude that the lattice deformation provided by the LCN substrate is the main driving force for the resonance tuning.

To further quantify the tuning capacity in plasmon resonance, Fig. 3c presents the center wavelengths of the transmission spectra at different excitation intensities. The resonance is shifted by 95 nm (from 1375 to 1280 nm) at the power range of 60–70 mW, indicating an abrupt nematic-to-isotropic phase transition of the LCN, which is accompanied by a large change in both the dimensions and the refractive index of the substrate. The power range at which this takes place is consistent with heat-induced spectral changes shown in ESI† Fig. S11. During excitation, the transmittance of the resonance peak remains essentially constant (Fig. 3c inset), inferring that there are no unexpected losses within the photoelastic metasurface

with and without the laser excitation. Moreover, the resonance of the photoelastic metasurface is spectrally shifted by 245 nm with the laser power of 90 mW, which corresponds to 70% of the FWHM of the initial resonance without excitation.

To characterize the reversibility of the photoelastic metasurface, transmission spectra are used to evaluate the performance after several switching-relaxation cycles. As shown in Fig. 3b, the center wavelength is blue shifted from 1490 nm to 1355 nm with laser excitation, and it returns to 1465 nm after ceasing the light, deviated from its original state. Fig. 3d elaborates the change of resonance during multiple excitation cycles, showing certain amount of irreversibility. Such decreasing trend in tuning ability may be ascribed to plastic deformation or topographic change of LCN material, as well as to dye bleaching during light excitation.

Light switchable polarization anisotropy

As illustrated in the inset of Fig. 3a, the uniaxial contraction of the LCN substrate induces anisotropy into the plasmonic nanostructure, which serves as a motivation for investigating the polarization dependence of the resonance wavelength and the transmittance upon photomechanical actuation. Fig. 4a presents a 3D transmittance plot at different probe polarization before the photoactuation. The resonance wavelength appears to be polarization-independent (blue curve in Fig. 4c), most
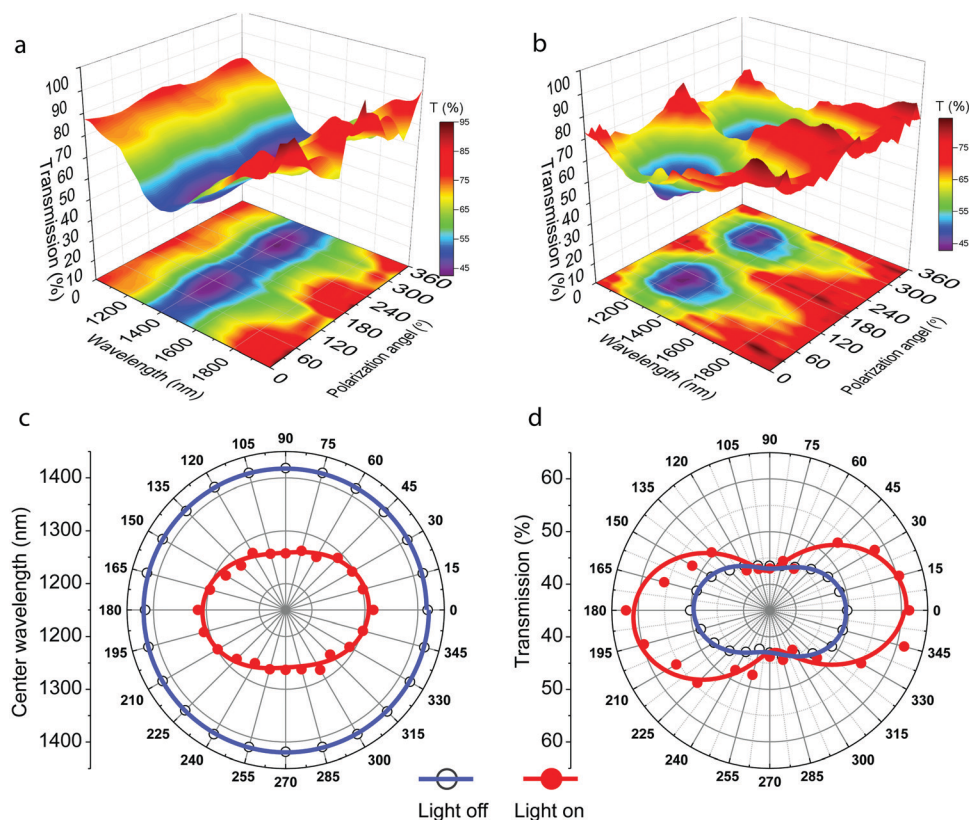

Fig. 4 Light switchable polarization sensitivity. (a and b) 3D surface plot of transmission spectra without (a) and with (b) photoelastic deformation. (c and d) Polar plots of extracted center wavelengths (c) and transmittance (d) for light off state (blue circles) and light on state (red dots). The excitation power of the control laser is fixed to 90 mW with spot size of 700 μm.

likely due to the fact that the polarization direction of the Au array is orthogonal to the orientation direction of the LC molecules within the LCN. A small anisotropy in transmittance is observed due to the birefringent nature of the LCN substrate (blue curve in Fig. 4d). Upon photomechanical deformation, the reshaped lattice gives rise to the change of resonance (Fig. 4b): the center wavelength (1310 nm and 1264 nm for 0 and 90° polarizations, respectively; red curve in Fig. 4c) and transmittance (42% to 63% for 0 to 90° polarization, respectively; red curve in Fig. 4d) both exhibit significant polarization dependence. This optically induced polarization dependence provides a new degree of freedom for controlling light-matter interactions in active metasurfaces. Importantly, the polarization of the incident beam is not only controlled by the structural anisotropy,[60] but also capable of being switched through another non-polarized excitation beam, which may be technically important for all-optical modulation devices.

A diffractive light modulator

The NSL-fabricated metasurface lattice produces hexagonal far-field diffraction pattern (Fig. 5a), offering a visible way to realize all-optical light modulation. We demonstrate this with the photoelastic metasurface, in which a continuous laser (633 nm, 1 mW) is used as a probe and a modulated 532 nm beam (60 mW, 0.1 Hz) for excitation. The optical setup and details of the measurement are given in ESI.† Within the hexagonal diffraction pattern, the distances between three adjacent spots are defined as a and b (top of Fig. 5a). Upon cyclic excitation, the lattice distances A and B (bottom of Fig. 5a) are modulated. Accordingly, a and b are alternately changed with a π phase shift, as shown in Fig. 5b. The relation between the metasurface lattice and the far-field diffraction pattern is calculated as shown in ESI† Fig. S12. Based on the light-controlled diffraction, the intensity at the far field receiver can be temporally controlled, for example, to synchronize the excitation beam (Fig. 5c). We examine the light-modulation process by using different pump powers with 0.1 Hz excitation frequency. During the light modulation, the rise time can be reduced from about 2 s (20 mW excitation) to below 1 s upon increasing the excitation power. The relaxation remains constant at *ca.* 1 s, irrespective of the excitation power, as dictated by the heat capacity of the LCN actuator upon photothermal excitation. Hence, to attain ultra-fast photomechanical tuning, scaling down the size of the photoelastic substrate would be required.[50] Details of the optical setups for microscopy spectra, far-field diffraction pattern and diffraction intensity measurements are shown in ESI† Fig. S15 and S16.

Discussion

The range of spectral tuning (between 1245 and 1490 nm) in this LCN-metasurface is ultra-large, by comparing to other results obtained by using different material systems and mechanisms, as specifically shown in ESI† Table S1. However, a high-performance tunable metasurface should possess large deformability of the actuating soft substrate and excellent mechanical stability to preserve the periodic nanostructure that dictates the resonance. To address the balance between softness and rigidity to obtain robust reversible tunability will be a long-term challenge. This study constitutes the first step towards photomechanical tuning of plasmon resonance on a deformable soft LCN substrate, with clear drawback in reversibility as brought out in Fig. 3d. At the same time, we highlight that both cyclic film deformation (ESI† Fig. S7) and diffraction modulation (Fig. 5c) show excellent reversibility. The irreversibility only comes to play in the resonance of the Au nanostructure, and it is ascribed to dye degradation and resultant reduction in absorption efficiency, surface wrinkling (ESI† Fig. S13), and irreversible topographic change of Au nanopattern that may be caused by the photothermal effect and further boosted by the local electric fields. For practical applications requiring large number of tuning cycles, significant improvement of the reversibility in the material shape changes is demanded. Replacing the glassy LCN with a liquid crystal elastomer[61] would yield a substrate with larger deformability at lower phase transition temperature together with higher resilience for shape relaxation, which could be a promising material platform for further improving the tuning capacity.

Even if NSL is used in this work to demonstrate large-area, low-cost metasurface fabrication, it is possible to extend the proposed concept to metasurfaces fabricated through standard UV exposure lithography. One example is shown in ESI† Fig. S14a, where a two-dimensional disk array (3 μm disk diameter) is obtained through mask exposure on the LCN film.
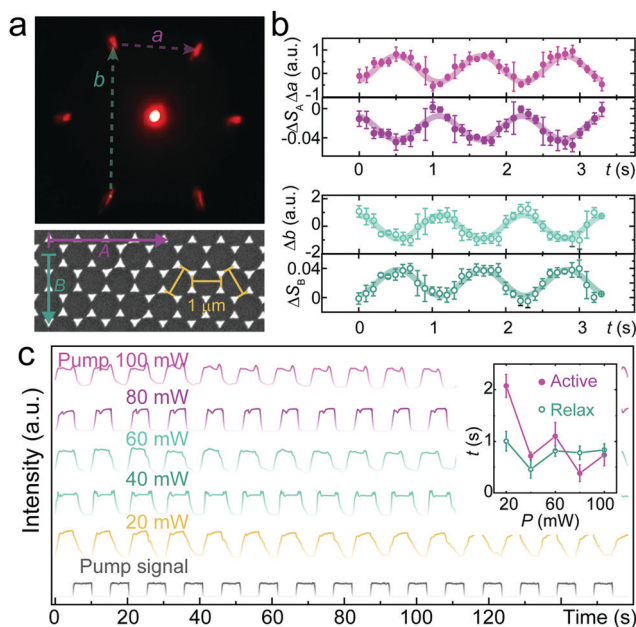

Fig. 5 Dynamic response of the diffraction and transmission under control laser modulation. (a) CCD image of the diffraction pattern (top) of the metasurface (bottom). (b) Length variation of distances a, b denoted in diffraction pattern and strains along A, B (S_A, S_B) directions in the metasurface lattice, upon temporally modulated laser excitation. (c) The temporal response of the transmitted signal with different intensity of the pump laser. The black line presents the trigger reference. Inset plots the active and relax speed.

The molecular orientation (dictating the substrate deformability) is well preserved in the LCN substrate (ESI† Fig. S14b and c), after treatment with RZX-3038 and acetone, two typical solvents used in standard lithographic processes. For further details on the fabrication steps, see ESI† Fig. S14d.

A photomechanically deformable metasurface, as represented in this work, is readily applicable for tunable metasurface holography,[35] where dynamic holographic images can be attained by laterally deforming the patterned substrate. However, for precise control of also the phase of the hologram, more strict positioning of the meta-units and the substrate deformation is required. Note that the topological deformation of the LCN substrate can be very versatile as it can be precisely programmed via patterning the director field,[48] and electron beam lithography can be used as a pathway to improve the structural accuracy. However, the inherent temperature deformability of the LCN substrate during the fabrication steps (e.g., baking of PMMA about 180 °C prior and post to the e-beam lithography) poses a technical challenge that must be taken into account in future investigations.

The straightforward dimensional control of polystyrene nanospheres or other self-assembled particles with distinct geometries offers a wide selection of metasurface lattice patterns and broad range of resonance wavelengths.[62–64] By tuning the resonance to the telecommunication band, our method may provide a potentially useful route to data encoding and interconnected optical communication. By shifting the resonance into the visible regime, primary-colored display devices can be envisioned.

To conclude, we demonstrate a photomechanically tunable metasurface based on light-responsive LCN substrate. The metasurface is capable of dynamic all-optical control in transmission through laterally deforming the nanoscale lattice. The resonance can be tuned across 245 nm spectral range in the near-IR region, while the polarization sensitivity can also be switched on–off through anisotropic photoelastic deformation. We also demonstrate an all-optical light modulator based on far-field diffraction raised from microscale periodic lattice. We believe that the results will inspire further studies on the proposed photomechanical platform for photonic applications. For instance, integration of the photoelastic metasurface with vertical cavity structures could provide tunable surface emitting structures and programmable lasing with controlled directionality.[65] The opportunities provided offer a prospective vision towards adaptive optics and reconfigurable photonics, in long term can be potentially useful for integrated optics and photonic communication.

Materials and methods

Sample preparation

The photoelastic metasurface consists of LCN substrate and gold nanoarray deposited on top of it. The LCN substrate was photopolymerized from a monomer mixture containing 78.5 mol% of LC monomer 4-methoxybenzoic acid 4-(6-acryloyloxyhexyloxy)phenyl ester (Synthon Chemicals), 20 mol% of LC crosslinker, 1,4-bis-[4-(6-acryloyloxyhexyloxy)benzoyloxy]-2-methylbenzene (Synthon Chemicals), 0.5 mol% Disperse Red 1 acrylate (Merck) and 1 mol% of photoinitiator (2,2-dimethoxy-2-phenylacetophenone, Sigma Aldrich). All molecules were used as received. The monomer mixture was polymerized by UV light (center wavelength of 365 nm, 60 mW cm^{-2}) at 50 °C in a cell with thickness of 45 μm. After opening the cell after the polymerization process, the LCN-adhered glass substrate was treated with UV ozone to increase the hydrophilicity and then used as the substrate to lift-up the self-assembled PS nanospheres. The PS nanosphere (Alpha Aesar Chemicals) layer was formed via the air–liquid interface method,[53,54] deposited on the LCN and served as a template mask for gold layer deposition (electron-beam evaporator, TF500, British HHV). After the deposition, the sample was soaked into water and treated with an ultrasonic cleaner to remove the PS nanospheres. The metasurface was stripped from the glass, and cut to small pieces for experiments.

Measurement procedure

The optical setup for measuring the transmission spectra, diffraction pattern, and temporal response can be found in ESI† Fig. S15 and S16. The transmission spectra were measured with CRAIC microspectrometer with reference signal taken from quartz substrate. The sample was ∼ 200 × 200 μm^2 and it was placed vertically to the probing beam from a broadband light source (70W Xenon lamp, Olympus) and the excitation laser (532 nm). The transmitted light was collected by a 10× objective lens (N.A. 0.25) and guided to camera and spectrometer with help of a beam splitter. CMOS camera was used to image the sample during in situ measurements. More details can be found from ESI.†

For the diffracted pattern characterization, the far-field diffraction pattern of a collimated continuous-wave probe laser (633 nm He–Ne laser, 1 mW) was analyzed while exciting the photoelastic metasurface with a pump laser (1 Hz pulsed 532 nm laser, 30 mW). A cropped sample with size of 5 × 5 mm^2 was placed on the displacement table to adjust the area for high-quality diffraction pattern. The pump laser beam was focused to a spot with size ∼ 700 μm. The diffraction pattern was imaged by a CMOS camera (msx1, Mshot) with frame rate of 11 fps. For the kinetics characterization, the pump laser (532 nm) is tuned with 0.1 Hz frequency. The transmitted light (633 nm He–Ne laser, 1 mW) was directly collected by a multimode fiber through a focus lens and guided to a spectrometer (USB2000 +, Ocean Optics).

Data availability

The data that support the findings of this study are available from the corresponding authors upon reasonable request.

Author contributions

Y. J. L., A. P. conceived the project; J. L. carried out experiments under supervision of H. Z. and Y. J. L.; J. L., H. Z., wrote the manuscript with input from others. All authors have

contributed in design of the work, analysis of data and given approval to the final version of the manuscript.

Conflicts of interest

The authors declare no competing interests.

Acknowledgements

References

1 N. Yu and F. Capasso, Flat optics with designer metasurfaces, *Nat. Mater.*, 2014, **13**(2), 139–150.

2 H. H. Hsiao, C. H. Chu and D. P. Tsai, Fundamentals and applications of metasurfaces, *Small Methods*, 2017, **1**(4), 1600064.

3 B. Sepulveda, P. C. Angelome, L. M. Lechuga and L. M. Liz-Marzan, LSPR-based nanobiosensors, *Nano Today*, 2009, **4**(3), 244–251.

4 B. Xiong, L. Deng, R. W. Peng and Y. M. Liu, Controlling the degrees of freedom in metasurface designs for multi-functional optical devices, *Nanoscale Adv.*, 2019, **1**(10), 3786–3806.

5 F. Qin, L. Ding, L. Zhang, F. Monticone, C. C. Chum, J. Deng, S. Mei, Y. Li, J. Teng, M. Hong, S. Zhang, A. Alu and C. W. Qiu, Hybrid bilayer plasmonic metasurface efficiently manipulates visible light, *Sci. Adv.*, 2016, **2**(1), e1501168.

6 Y. J. Liu, H. Liu, E. S. P. Leong, C. C. Chum and J. H. Teng, Fractal holey metal microlenses with significantly suppressed side lobes and high-order diffractions in focusing, *Adv. Opt. Mater.*, 2014, **2**(5), 487–492.

7 G. Zheng, H. Muhlenbernd, M. Kenney, G. Li, T. Zentgraf and S. Zhang, Metasurface holograms reaching 80% efficiency, *Nat. Nanotechnol.*, 2015, **10**(4), 308–312.

8 M. S. Bin-Alam;, O. Reshef;, Y. Mamchur;, M. Z. Alam;, G. Carlow;, J. Upham;, B. T. Sullivan;, J. M. Menard;, M. J. Huttunen;, R. W. Boyd; and K. Dolgaleva, Ultra-high-Q resonances in plasmonic metasurfaces, *Nat. Commun.*, 2021, **12**(1), 974.

9 X. Zhu, C. Vannahme, E. Hojlund-Nielsen, N. A. Mortensen and A. Kristensen, Plasmonic colour laser printing, *Nat. Nanotechnol.*, 2016, **11**(4), 325–329.

10 N. Jiang, X. Zhuo and J. Wang, Active plasmonics: principles, structures, and applications, *Chem. Rev.*, 2018, **118**(6), 3054–3099.

11 L. Zhu, J. Kapraun, J. Ferrara and C. J. Chang-Hasnain, Flexible photonic metastructures for tunable coloration, *Optica*, 2015, **2**(3), 255–258.

12 D. Franklin, Y. Chen, A. Vazquez-Guardado, S. Modak, J. Boroumand, D. Xu, S. T. Wu and D. Chanda, Polarization-independent actively tunable colour generation on imprinted plasmonic surfaces, *Nat. Commun.*, 2015, **6**, 7337.

13 L. Bao and T. J. Cui, Tunable, reconfigurable, and program-mable metamaterials, *Microw. Opt. Technol. Lett.*, 2020, **62**(1), 9–32.

14 C. W. Lee, H. J. Choi and H. Jeong, Tunable metasurfaces for visible and SWIR applications, *Nano Convergence*, 2020, **7**(1), 1–11.

15 A. Angelini, F. Pirani, F. Frascella and E. Descrovi, Reconfigurable elastomeric graded-index optical elements controlled by light, *Light: Sci. Appl.*, 2018, **7**(1), 1–9.

16 L. Michaeli, H. Suchowski and T. Ellenbogen, Near-infrared tunable surface lattice induced transparency in a plasmonic metasurface, *Laser Photonics Rev.*, 2019, **14**(1), 1900204.

17 A. She, S. Zhang, S. Shian, D. R. Clarke and F. Capasso, Adaptive metalenses with simultaneous electrical control of focal length, astigmatism, and shift, *Sci. Adv.*, 2018, **4**(2), eaap9957.

18 E. Arbabi, A. Arbabi, S. M. Kamali, Y. Horie, M. Faraji-Dana and A. Faraon, MEMS-tunable dielectric metasurface lens, *Nat. Commun.*, 2018, **9**(1), 1–9.

19 S. C. Malek, A. C. Overvig, S. Shrestha and N. F. Yu, Active nonlocal metasurfaces, *Nanophotonics*, 2021, **10**(1), 655–665.

20 A. M. Shaltout, V. M. Shalaev and M. L. Brongersma, Spatiotemporal light control with active metasurfaces, *Science*, 2019, **364**(6441), eaat3100.

21 Y. Liu, K. Tom, X. Wang, C. Huang, H. Yuan, H. Ding, C. Ko, J. Suh, L. Pan, K. A. Persson and J. Yao, Dynamic control of optical response in layered metal chalcogenide nanoplates, *Nano Lett.*, 2016, **16**(1), 488–496.

22 Y. W. Huang, H. W. H. Lee, R. Sokhoyan, R. P. Pala, K. Thyagarajan, S. Han, D. P. Tasi and H. A. Atwater, Gate-tunable conducting oxide metasurfaces, *Nano Lett.*, 2016, **16**(9), 5319–5325.

23 G. K. Shirmanesh, R. Sokhoyan, P. C. Wu and H. A. Atwater, Electro-optically tunable multifunctional metasurfaces, *ACS Nano*, 2020, **14**(6), 6912–6920.

24 S. M. Kamali, E. Arbabi, A. Arbabi, Y. Horie and A. Faraon, Highly tunable elastic dielectric metasurface lenses, *Laser Photonics Rev.*, 2016, **10**(6), 1002–1008.

25 A. Shaltout, A. Kildishev and V. Shalaev, Time-varying metasurfaces and Lorentz non-reciprocity, *Opt. Mater. Express*, 2015, **5**(11), 2459–2467.

26 J. Shabanpour, Programmable anisotropic digital metasurface for independent manipulation of dual-polarized THz

waves based on a voltage-controlled phase transition of VO2 microwires, *J. Mater. Chem. C*, 2020, **8**(21), 7189–7199.

27 Z. Shao, X. Cao, H. Luo and P. Jin, Recent progress in the phase-transition mechanism and modulation of vanadium dioxide materials, *NPG Asia Mater.*, 2018, **10**(7), 581–605.

28 X. Yin, T. Steinle, L. Huang, T. Taubner, M. Wuttig, T. Zentgraf and H. Giessen, Beam switching and bifocal zoom lensing using active plasmonic metasurfaces, *Light: Sci. Appl.*, 2017, **6**(7), e17016.

29 M. X. Ren, W. Wu, W. Cai, B. Pi, X. Z. Zhang and J. J. Xu, Reconfigurable metasurfaces that enable light polarization control by light, *Light: Sci. Appl.*, 2017, **6**(6), e16254.

30 Y. J. Liu, G. Y. Si, E. S. Leong, N. Xiang, A. J. Danner and J. H. Teng, Light-driven plasmonic color filters by overlaying photoresponsive liquid crystals on gold annular aperture arrays, *Adv. Mater.*, 2012, **24**(23), OP131–OP135.

31 S. Geiger, J. Michon, S. Liu, J. Qin, J. Ni, J. Hu, T. Gu and N. Lu, Flexible and stretchable photonics: the next stretch of opportunities, *ACS Photonics*, 2020, **7**(10), 2618–2635.

32 W. Chen, W. Liu, Y. Jiang, M. Zhang, N. Song, N. J. Greybush, J. Guo, A. K. Estep, K. T. Turner, R. Agarwal and C. R. Kagan, Ultrasensitive, mechanically responsive optical metasurfaces via strain amplification, *ACS Nano*, 2018, **12**(11), 10683–10692.

33 M. L. Tseng, J. Yang, M. Semmlinger, C. Zhang, P. Nordlander and N. J. Halas, Two-dimensional active tuning of an aluminum plasmonic array for full-spectrum response, *Nano Lett.*, 2017, **17**(10), 6034–6039.

34 H. S. Ee and R. Agarwal, Tunable metasurface and flat optical zoom lens on a stretchable substrate, *Nano Lett.*, 2016, **16**(4), 2818–2823.

35 S. C. Malek, H. S. Ee and R. Agarwal, Strain multiplexed metasurface holograms on a stretchable substrate, *Nano Lett.*, 2017, **17**(6), 3641–3645.

36 F. Cheng, L. Qiu, D. Nikolov, A. Bauer, J. P. Rolland and A. N. Vamivakas, Mechanically tunable focusing metamirror in the visible, *Opt. Express*, 2019, **27**(11), 15194–15204.

37 Y. F. Liu, R. Zhang and P. V. Braun, Mechanical deformation–assisted fabrication of plasmonic nanobowties with broken symmetry and tunable gaps, *Part. Part. Syst. Charact.*, 2019, **37**(2), 1900463.

38 D. Mistry, S. D. Connell, S. L. Mickthwaite, P. B. Morgan, J. H. Clamp and H. F. Gleeson, Coincident molecular auxeticity and negative order parameter in a liquid crystal elastomer, *Nat. Commun.*, 2018, **9**(1), 5095.

39 T. Seki, New strategies and implications for the photoalignment of liquid crystalline polymers, *Polym. J.*, 2014, **46**(11), 751–768.

40 T. J. White and D. J. Broer, Programmable and adaptive mechanics with liquid crystal polymer networks and elastomers, *Nat. Mater.*, 2015, **14**(11), 1087–1098.

41 K. Urayama, S. Honda and T. Takigawa, Deformation coupled to director rotation in swollen nematic elastomers under electric fields, *Macromolecules*, 2006, **39**(5), 1943–1949.

42 A. Kaiser, M. Winkler, S. Krause, H. Finkelmann and A. M. Schmidt, Magnetoactive liquid crystal elastomer nanocomposites, *J. Mater. Chem.*, 2009, **19**(4), 538–543.

43 Z. Yan, X. Ji, W. Wu, J. Wei and Y. Yu, Light-switchable behavior of a microarray of azobenzene liquid crystal polymer induced by photodeformation, *Macromol. Rapid Commun.*, 2012, **33**(16), 1362–1367.

44 H. Zeng, P. Wasylczyk, D. S. Wiersma and A. Priimagi, Light robots: bridging the gap between microrobotics and photomechanics in soft materials, *Adv. Mater.*, 2018, **30**(24), e1703554.

45 X. Y. Liu, R. B. Wei, P. T. Hoang, X. G. Wang, T. Liu and P. Keller, Reversible and rapid laser actuation of liquid crystalline elastomer micropillars with inclusion of gold nanoparticles, *Adv. Funct. Mater.*, 2015, **25**(20), 3022–3032.

46 H. Zeng, M. Lahikainen, L. Liu, Z. Ahmed, O. M. Wani, M. Wang, H. Yang and A. Priimagi, Light-fuelled freestyle self-oscillators, *Nat. Commun.*, 2019, **10**(1), 5057.

47 A. Habibpourmoghadam, L. Wolfram, F. Jahanbakhsh, B. Mohr, V. Y. Reshetnyak and A. Lorenz, Tunable diffraction gratings in copolymer network liquid crystals driven with interdigitated electrodes, *ACS Appl. Electron. Mater.*, 2019, **1**(12), 2574–2584.

48 G. Babakhanova, T. Turiv, Y. Guo, M. Hendrikx, Q. H. Wei, A. Schenning, D. J. Broer and O. D. Lavrentovich, Liquid crystal elastomer coatings with programmed response of surface profile, *Nat. Commun.*, 2018, **9**(1), 456.

49 A. M. Flatae, M. Burresi, H. Zeng, S. Nocentini, S. Wiegele, C. Parmeggiani, H. Kalt and D. Wiersma, Optically controlled elastic microcavities, *Light: Sci. Appl.*, 2015, **4**(4), e282–e282.

50 S. Nocentini, D. Martella, C. Parmeggiani, S. Zanotto and D. S. Wiersma, Structured optical materials controlled by light, *Adv. Opt. Mater.*, 2018, **6**(15), 1800167.

51 Y. B. Guo, H. Shahsavan and M. Sitti, Microscale polarization color pixels from liquid crystal elastomers, *Adv. Opt. Mater.*, 2020, **8**(17), 1902098.

52 S. Woska, A. Münchinger, D. Beutel, E. Blasco, J. Hessenauer, O. Karayel, P. Rietz, S. Pfleging, R. Oberle, C. Rockstuhl, M. Wegener and H. Kalt, Tunable photonic devices by 3D laser printing of liquid crystal elastomers, *Opt. Mater. Express*, 2020, **10**(11), 2928–2943.

53 Z. Wang, J. Liu, X. Fang, J. Wang, Z. Yin, H. He, S. Jiang, M. Zhao, Z. Yin, D. Luo, P. Shum and Y. J. Liu, Plasmonically enhanced photoluminescence of monolayer MoS2 via nanosphere lithography-templated gold metasurfaces, *Nanophotonics*, 2021, **10**(6), 1733–1740.

54 X. Fang, C. Zheng, Z. Yin, Z. Wang, J. Wang, J. Liu, D. Luo and Y. J. Liu, Hierarchically ordered silicon metastructures from improved self-assembly-based nanosphere lithography, *ACS Appl. Mater. Interfaces*, 2020, **12**(10), 12345–12352.

55 C. Ohm, M. Brehmer and R. Zentel, Liquid crystalline elastomers as actuators and sensors, *Adv. Mater.*, 2010, **22**, 3366–3387.

56 O. Reshef, M. Saad-Bin-Alam, M. J. Huttunen, G. Carlow, B. T. Sullivan, J. M. Menard, K. Dolgaleva and R. W. Boyd, Multiresonant high-Q plasmonic metasurfaces, *Nano Lett.*, 2019, **19**(9), 6429–6434.

57 V. Amendola, R. Pilot, M. Frasconi, O. M. Marago and M. A. Iati, Surface plasmon resonance in gold nanoparticles: a review, *J. Phys.: Condens. Matter*, 2017, **29**(20), 203002.

58 J. Li and S. T. Wu, Infrared refractive indices of liquid crystals, *J. Appl. Phys.*, 2005, **97**(7), 073501.

59 S. T. Wu, Birefringence dispersions of liquid crystals, *Phys. Rev. A: At., Mol., Opt. Phys.*, 1986, **33**(2), 1270.

60 J. Park, J. H. Kang, S. J. Kim, X. Liu and M. L. Brongersma, Dynamic reflection phase and polarization control in meta-surfaces, *Nano Lett.*, 2017, **17**(1), 407–413.

61 M. O. Saed, C. P. Ambulo, H. Kim, R. De, V. Raval, K. Searles, D. A. Siddiqui, J. M. O. Cue, M. C. Stefan, M. R. Shankar and T. H. Ware, Molecularly-engineered, 4D-printed liquid crystal elastomer actuators, *Adv. Funct. Mater.*, 2019, **29**(3), 1806412.

62 A. Kuzyk, R. Jungmann, G. P. Acuna and N. Liu, DNA origami route for nanophotonics, *ACS Photonics*, 2018, **5**(4), 1151–1163.

63 X. Liang, R. Dong and J. C. Ho, Self-assembly of colloidal spheres toward fabrication of hierarchical and periodic nanostructures for technological applications, *Adv. Mater. Technol.*, 2019, **4**(3), 1800541.

64 K. Chen, B. B. Rajeeva, Z. Wu, M. Rukavina, T. D. Dao, S. Ishii, M. Aono, T. Nagao and Y. Zheng, Moire nanosphere lithography, *ACS Nano*, 2015, **9**(6), 6031–6040.

65 Y. Y. Xie, P. N. Ni, Q. H. Wang, Q. Kan, G. Briere, P. P. Chen, Z. Z. Zhao, A. Delga, H. R. Ren, H. D. Chen, C. Xu and P. Genevet, Metasurface-integrated vertical cavity surface-emitting lasers for programmable directional lasing emissions, *Nat. Nanotechnol.*, 2020, **15**(2), 125–130.